

# Barycenteric distribution alignment and manifold-restricted invertibility for domain generalization

Boyang Lyu<sup>1</sup>, Thuan Nguyen<sup>1,3</sup>, Prakash Ishwar<sup>2</sup>, Matthias Scheutz<sup>3</sup>, Shuchin Aeron<sup>1\*</sup>

November 24, 2021

## Abstract

For the Domain Generalization (DG) problem where the hypotheses are composed of a common representation function followed by a labeling function, we point out a shortcoming in existing approaches that fail to explicitly optimize for a term, appearing in a well-known and widely adopted upper bound to the risk on the unseen domain, that is dependent on the representation to be learned. To this end, we first derive a novel upper bound to the prediction risk. We show that imposing a mild assumption on the representation to be learned, namely manifold restricted invertibility that is known to be satisfied by many datasets, is sufficient to deal with this issue. Further, unlike existing approaches, our novel upper bound doesn't require the assumption of Lipschitzness of the loss function. In addition, the distributional discrepancy in the representation space is handled via the Wasserstein-2 barycenter cost. In this context, we creatively leverage old and recent *transport inequalities*, which link various optimal transport metrics, in particular the  $L^1$  distance (also known as the total variation distance) and the Wasserstein-2 distances, with the Kullback-Liebler divergence. These analyses and insights motivate a new representation learning cost for DG that additively balances three competing objectives: 1) minimizing classification error across seen domains via cross entropy, 2) enforcing domain-invariance in the representation space via the Wasserstein-2 barycenter cost, and 3) promoting non-degenerate, nearly-invertible representation via one of two mechanisms, viz., an autoencoder-based reconstruction loss or a mutual information loss. It is to be noted that the proposed algorithms completely bypass the use of any adversarial training mechanism that is typical of many current domain generalization approaches. Simulation results on several standard datasets demonstrate superior performance compared to several well-known DG algorithms.

## 1 Introduction

In many practical applications of modern machine learning, the training (seen) data and the test (unseen) data may belong to different *domains*, leading to loss of predictive power of the learned models. For example, a model trained on data from one hospital may not work well when the test data is from

---

<sup>1</sup> - Tufts University, Dept. of ECE, <sup>2</sup> - Boston University, Dept. of ECE, <sup>3</sup> - Tufts University, Dept of CS.

**Corresponding authors:** Boyang Lyu, email: [Boyang.Lyu@tufts.edu](mailto:Boyang.Lyu@tufts.edu).

another hospital [Gulrajani and Lopez-Paz, 2020], a drowsiness driving estimator trained on one group of subjects does not generalize well for other subjects [Cui et al., 2019], a cognitive workload estimator from fNIRS (Fourier Near-Infrared Sensor) measurements may not generalize well across sessions and subjects [Lyu et al., 2021].

These types of problems are broadly classified into two categories, viz., Domain Adaptation (DA) [Ben-David et al., 2007] and Domain Generalization (DG) [Blanchard et al., 2011]. Both DA and DG aim to find a model that can generalize well when the seen domain training data does not share the same distribution with the testing data from the unseen domain. The key difference between DA and DG is that DA allows access to the (unlabeled) unseen domain data during the training process while DG does not, leading to a more challenging problem. For an extensive survey and related literature on these two topics we refer the reader to excellent recent surveys [Wang et al., 2021, Zhou et al., 2021b] for DG, and [Redko et al., 2020] for DA.

To address the problem of DG, in practice, one usually parameterizes the hypothesis as composed of a representation function followed by a labeling function [Albuquerque et al., 2019, Dou et al., 2019, Li et al., 2018b, Zhou et al., 2021a]. This approach has its roots in the seminal works of [Ben-David et al., 2007, 2010], where the upper bounds on the risk of unseen domain were derived for the simple but instructive binary classification setting. The essential insight from the upper bound derived in [Ben-David et al., 2007, 2010] is that the risk on the unseen domain is upper bounded by three terms: (1) the prediction risk on the mixture of seen domains, (2) discrepancy or divergence between the data distributions in the representation space, and (3) a *combined risk* across all domains that depends on the representation map. While most of the existing work ignores optimizing the third term (combined risk) and treats it as a constant for a given representation map (for example, Theorem 1 in [Ben-David et al., 2010]), that term is actually a function of the representation map, and hence needs to be part of the optimization. Ignoring this last but crucial subtlety, a large body of the DG (as well as DA) methods [Ajakan et al., 2014, Ganin et al., 2016, Zhao et al., 2018, 2019] are essentially based on a variation of the following theme - learn a domain invariant representation mapping *or* align the domains in the representation space, while learning a common labeling function controlling the prediction loss across the seen domains.

**Contributions:** To address the shortcoming discussed above, we revisit the main problem and derive a new upper bound in the representation space by invoking the now popular manifold hypothesis [Lei et al., 2020] that most data distributions are concentrated on low dimensional manifolds. Specifically, we make the mild assumption that the class of representation mappings are (nearly) invertible when restricted to distributions that lie on low-dimensional manifolds. Under this assumption, we derive a new upper bound for the risk in the representation space comprising three terms: (1) the prediction risk across seen domains in the input space; (2) the discrepancy/divergence between the induced distributions of seen and unseen domains in representation space that can be expressed in terms of the Wasserstein-2 Barycenter [Santambrogio, 2015] of the seen domains. For this we leverage old and new *transport inequalities* which also help do away with an additional Lipschitz assumption on the loss function typically assumed in related works; and (3) a *combined risk* that is truly independent of both the representation mapping and the labeling function. A detailed comparison between previous

bounds and our work can be found in Appendix A.1.

Our (manifold-restricted) invertibility assumption provides a natural justification for the use of an auto-encoder-like mechanism, which to date had been heuristically motivated in [Li et al., 2018b, Ghifary et al., 2015]. Moreover, to avoid introducing additional parameters to train for, namely the decoder, we propose the use of mutual information between the data and the representation as a surrogate for enforcing the approximate invertibility of the representation map.

Finally, based on these theoretical insights, we propose two novel algorithms, namely Wasserstein Barycenter Auto-Encoder (WBAE) and Wasserstein Barycenter Mutual Information (WBMI). The proposed algorithms leverage recent advances in the fast and efficient computation of Wasserstein barycenters as well as advances in computing reliable gradients of mutual information loss for implicit models from samples. We also note that the proposed algorithms completely bypass the use of any adversarial mechanism for domain alignment in the representation space.

**Related work:** In [Albuquerque et al., 2019], the authors propose a model consisting of three parts: a feature extractor, a classifier, and domain discriminators. The feature extractor learns the task-sensitive but domain-invariant feature via minimizing the cross entropy loss w.r.t the task label and maximizing the sum of domain discriminator loss. The domain discriminator loss is treated as an estimation of  $\mathcal{H}$  divergence [Ben-David et al., 2010] between all source domains. Zhou et al. [2020] use the pairwise Wasserstein-1 distance [Santambrogio, 2015, Peyré and Cuturi, 2019], to estimate the divergence between different source domains. Utilizing the dual form of the Wasserstein-1 distance, the feature extractor then minimizes a combination of cross entropy loss, Wasserstein distance loss, and a contrastive loss to achieve DG. Dou et al. [2019] adopt a gradient-based episodic training scheme for DG, with extracted features keeping the structure of the class relationship and the task-related clusters via minimization of alignment loss of soft-confusion matrix and a contrastive loss [van den Oord et al., 2018]. For an in-depth and comprehensive survey of such methods, we refer the reader to the excellent Appendix A.1 of [Gulrajani and Lopez-Paz, 2020].

## 2 Theoretical analysis and proposed methods

A *domain*  $v$  is a triple  $(\mu^{(v)}, f^{(v)}, g^{(v)})$  consisting of a distribution  $\mu^{(v)}$  on the inputs  $\mathbf{x} \in \mathbb{R}^d$ , a representation function  $f^{(v)} : \mathbb{R}^d \rightarrow \mathbb{R}^{d'}$  where  $d' \leq d$ , and a stochastic labeling function  $g^{(v)} : \mathbb{R}^{d'} \rightarrow \mathcal{Y}$  mapping the representation space to label space  $\mathcal{Y}$ . We denote the unseen domain by  $(\mu^{(u)}, f^{(u)}, g^{(u)})$  and the  $S$  seen domains by  $(\mu^{(s)}, f^{(s)}, g^{(s)})$ ,  $s = 1, \dots, S$ .

Let  $\mathcal{F} = \{f | f : \mathbb{R}^d \rightarrow \mathbb{R}^{d'}\}$  be a set of *representation functions*,  $\mathcal{G} = \{g | g : \mathbb{R}^{d'} \rightarrow \mathcal{Y}\}$  a set of stochastic *labeling functions*, and  $\mathcal{H} := \mathcal{G} \circ \mathcal{F}$  the set of *hypothesis*  $h : \mathbb{R}^d \rightarrow \mathcal{Y}$  obtained by composing each  $g \in \mathcal{G}$  with each  $f \in \mathcal{F}$ , i.e.,  $h = g \circ f$ .

Define the risk of using a hypothesis  $h$  in domain  $v$  by:

$$R^{(v)}(h) := \mathbb{E}_{\mathbf{x} \sim \mu^{(v)}} [\ell(h(\mathbf{x}), h^{(v)}(\mathbf{x}))] \quad (1)$$

where  $\mathbb{E}[\cdot]$  denotes expectation and  $h^{(v)} = g^{(v)} \circ f^{(v)}$ , and  $\ell(\cdot, \cdot)$  is a loss function. We make the following modeling assumptions:

**A1:**  $\ell(\cdot, \cdot)$  is non-negative, symmetric, bounded by a finite positive number  $L$ , and satisfies the triangle inequality.

**A2:** The representation function  $f$  is invertible when restricted to the intrinsically low-dimensional data manifold.

Assumption A1 can be easily satisfied by any metric or norm truncated by a finite positive number. Concretely, if  $d(a, b)$  is a metric, potentially unbounded like Mean Squared Error (MSE), then  $\text{loss}(a, b) := \min(L, d(a, b))$  satisfies A1. In contrast to our requirements, the loss function in [Redko et al., 2017] is supposed to be convex, symmetric, bounded, obeying the triangle inequality, and satisfying a specific form, while the loss function in [Shen et al., 2018] required to be Lipschitz with respect to the hypothesis due to the use of Wasserstein-1 distance.

Assumption A2 can be explained by the manifold hypothesis that real-world data like images lie in a low-dimensional manifold within a high-dimensional space, which is also the basis of most dimension-reducing mappings such as those based on classical PCA, auto-encoders, etc.. Thus, the dimensional-reducing mapping  $f$  can be exactly invertible or nearly so when restricted to an intrinsically low-dimensional data manifold embedded within the high-dimensional ambient space. The same phenomena and its application can also be seen in compressive sampling. For example, it is possible to recover a sparse high dimensional signal which belongs to the union of sub-spaces - a low-dimensional manifold, from a compressed low-dimensional linear mapping. Additionally, note that the success of Generative Adversarial Networks (GAN) [Goodfellow et al., 2014] is also based on transforming a low-dimensional Gaussian to a distribution on a manifold embedded within an ambient space of high dimension. In practice, invertibility can be approximately achieved if there exists a reconstruction map with a sufficiently low reconstruction error or if the mutual information between the input and its representation is large enough.

The rest of Section 2 is arranged as follows: In Section 2.1 we upper bound the unseen domain risk of a hypothesis in terms of its seen domain risks, the Wasserstein distance between the distributions of input representations of the hypothesis from the seen and unseen domains, and a term that is free of the representation and labeling functions of the hypothesis. In Section 2.2 we use the bounds derived in Section 2.1 to motivate the use of a new cost function for learning a hypothesis from labeled examples of all seen domain.

## 2.1 Bounds relating seen and unseen domain risks

We begin by considering a single seen domain. Lemma 1 below upper bounds the risk  $R^{(u)}(h)$  of a hypothesis  $h = g \circ f$  in the unseen domain  $u$  in terms of three terms: 1) its risk  $R^{(s)}(h)$  in a *single* seen domain  $s$ , 2) the  $L^1$  distance between the distributions of the *representations* of data from the seen and unseen domain, and 3) a third term  $\sigma^{(u,s)}$  that is free of  $h$  and is intrinsic to the domains and the loss function. We use the notation  $f_{\#}\mu^{(v)}$  to denote the pushforward of distribution of  $\mu^{(v)}$ , i.e., the distribution of  $f(\mathbf{x})$  with  $\mathbf{x} \sim \mu^{(v)}$ .

**Lemma 1.** For any hypothesis  $h \in \mathcal{H}$ ,

$$R^{(u)}(h) \leq R^{(s)}(h) + L \|f_\# \mu^{(u)} - f_\# \mu^{(s)}\|_1 + \sigma^{(u,s)} \quad (2)$$

where  $\|f_\# \mu^{(u)} - f_\# \mu^{(s)}\|_1 = \int (f_\# \mu^{(u)} - f_\# \mu^{(s)}) d\mathbf{x}$  denotes the  $L^1$  distance between  $(f_\# \mu^{(u)}, f_\# \mu^{(s)})$  and:

$$\sigma^{(u,s)} := \min \left\{ \mathbb{E}_{\mathbf{x} \sim \mu^{(u)}} [\ell(h^{(u)}(\mathbf{x}), h^{(s)}(\mathbf{x}))], \mathbb{E}_{\mathbf{x} \sim \mu^{(s)}} [\ell(h^{(u)}(\mathbf{x}), h^{(s)}(\mathbf{x}))] \right\}. \quad (3)$$

*Proof.* Please see Appendix A.2.  $\square$

The proposed upper bound in Lemma 1 requires  $f$  to be invertible. Particularly, the invertibility assumption is employed in the proof of Lemma 1, Eq. (25), Appendix A.2. This condition can be relaxed to nearly invertible as discussed in Appendix A.3, and implemented by minimizing reconstruction loss or maximizing the mutual information between representation and the input data as discussed in Section 2.2.

In typical applications of DG, training data from multiple seen domains are available which can be mixed together in myriad ways. Lemma 2 below therefore extends Lemma 1 to a convex combination of distributions of seen domains.

**Lemma 2.** For all convex weights  $\lambda^{(1)}, \lambda^{(2)}, \dots, \lambda^{(S)}$  (nonnegative and summing to one) and any hypothesis  $h \in \mathcal{H}$ ,

$$R^{(u)}(h) \leq \sum_{s=1}^S \lambda^{(s)} R^{(s)}(h) + L \sum_{s=1}^S \lambda^{(s)} \|f_\# \mu^{(u)} - f_\# \mu^{(s)}\|_1 + \sum_{s=1}^S \lambda^{(s)} \sigma^{(u,s)}. \quad (4)$$

*Proof.* This follows immediately by taking the convex combination of the bound given by Lemma 1 over the seen domains.  $\square$

The upper bound is based on the  $L^1$  distances between the pushforwards of seen and unseen distributions. Estimating  $L^1$  distances accurately from samples is well-known to be hard [Batu et al., 2000, Ben-David et al., 2010, Kifer et al., 2004]. To overcome this practical limitation, we upper bound the  $L^1$  distance by the Wasserstein-2 distance under additional regularity assumptions on the pushforwards.

**Definition 1.** [Polyanskiy and Wu, 2016] A probability distribution on  $\mathbb{R}^d$  is called  $(c_1, c_2)$ -regular, with  $c_1, c_2 \geq 0$ , if it is absolutely continuous with respect to the Lebesgue measure with a differentiable density  $p(\mathbf{x})$  such that

$$\forall \mathbf{x} \in \mathbb{R}^d, \quad \|\nabla \log_2 p(\mathbf{x})\|_2 \leq c_1 \|\mathbf{x}\|_2 + c_2,$$

where  $\nabla$  denotes the gradient and  $\|\cdot\|_2$  denotes the standard Euclidean norm.

**Lemma 3.** If  $\mu$  and  $\nu$  are  $(c_1, c_2)$ -regular, then

$$\|\mu - \nu\|_1 \leq \sqrt{c_1 \left( \sqrt{\mathbb{E}_{\mathbf{u} \sim \mu} [\|\mathbf{u}\|_2^2]} + \sqrt{\mathbb{E}_{\mathbf{v} \sim \nu} [\|\mathbf{v}\|_2^2]} \right) + 2c_2} \quad [\mathbb{W}_2(\mu, \nu)]^{1/2}, \quad (5)$$

where,  $\mathbb{W}_p(\mu, \nu)$  denotes the Wasserstein- $p$  metric [Peyré and Cuturi, 2019, Santambrogio, 2015, Villani, 2003] defined as,

$$\mathbb{W}_p(\mu, \nu) := \min_{\pi \in \Pi(\mu, \nu)} (\mathbb{E}_{(\mathbf{u}, \mathbf{v}) \sim \pi} [\|\mathbf{u} - \mathbf{v}\|_2^p])^{1/p},$$

where  $\Pi(\mu, \nu)$  is the set of joint distributions with marginals  $\mu$  and  $\nu$ .

*Proof.* Please see Appendix A.4.  $\square$

The key question is what conditions guarantee the regularity of the pushforward distributions? Proposition 2 and Proposition 3 in [Polyanskiy and Wu, 2016] show that any distribution  $\nu$  for which  $\mathbb{E}_{\mathbf{v} \sim \nu} \|\mathbf{v}\|_2$  is finite becomes regular when convolved with any regular distribution, including the Gaussian distribution. Since convolution of distributions corresponds to addition of independent random vectors having those distributions, in practice it is always possible to make the pushforwards regular by adding a small amount of independent spherical Gaussian noise in representation space.

Combining Lemma 2, Lemma 3, and Jensen's inequality, we obtain our main result:

**Theorem 1.** *If  $f_\# \mu^{(s)}$ ,  $s = 1, 2, \dots, S$ , and  $f_\# \mu^{(u)}$  are all  $(c_1, c_2)$ -regular, then for all convex weights  $\lambda^{(1)}, \lambda^{(2)}, \dots, \lambda^{(S)}$  and any hypothesis  $h \in \mathcal{H}$ ,*

$$R^{(u)}(h) \leq \sum_{s=1}^S \lambda^{(s)} R^{(s)}(h) + LC \left[ \sum_{s=1}^S \lambda^{(s)} \mathbb{W}_2^2(f_\# \mu^{(u)}, f_\# \mu^{(s)}) \right]^{1/4} + \sum_{s=1}^S \lambda^{(s)} \sigma^{(u,s)} \quad (6)$$

where

$$C = \max_{s \in \{1, \dots, S\}} \sqrt{c_1 \left( \sqrt{\mathbb{E}_{\mathbf{x} \sim \mu^{(u)}} [\|f(\mathbf{x})\|^2]} + \sqrt{\mathbb{E}_{\mathbf{x} \sim \mu^{(s)}} [\|f(\mathbf{x})\|^2]} \right) + 2c_2}. \quad (7)$$

*Proof.* Please see Appendix A.5.  $\square$

It is worth noting that the third term  $\sum_{s=1}^S \lambda^{(s)} \sigma^{(u,s)}$  in the upper bound of Theorem 1 is independent from both the representation map  $f$  and the labeling function  $g$  that contrasts to the previous results in [Ben-David et al., 2007], please see our detailed analysis in Appendix A.1. In addition, even though the form of the upper bound derived above shares some similarities with Lemma 1 in [Redko et al., 2017] and Theorem 1 in [Shen et al., 2018], for example, all of them introduce Wasserstein distance between domain distributions, the content is indeed different from previous work based on the following key points.

1. Our upper bound is constructed in the *representation* space and not in the data (ambient) space, which provides a theoretical justification for the risk of unseen domain when decomposing the hypothesis into a representation mapping and a labeling function. This is also consistent with the algorithm implementation in practice.
2. The loss function in [Redko et al., 2017] is assumed to be convex, symmetric, bounded, obeying the triangle inequality, and satisfying a specific form, while in [Shen et al., 2018], it is required to be Lipschitz with respect to the hypothesis due to the use of Wasserstein-1 distance. With less constraints posed on the loss function, we only assume it is symmetric, bounded, and satisfies triangle inequality.

3. The bounds in Lemma 1 of [Redko et al., 2017] and Theorem 1 of [Shen et al., 2018] are controlled by the Wasserstein-1 distance while our upper bound is managed by the square-root of the Wasserstein-2 distance. At the first glance, it is hard to conclude which upper bound is tighter and in general, there are regimes where one bound is tighter than the other. First, it is well-known that  $W_1(\mu, \nu) \leq W_2(\mu, \nu)$  for two arbitrary distributions  $\mu$  and  $\nu$ . Therefore, if  $W_2(\mu, \nu) \leq 1$ , one can conclude that  $W_1(\mu, \nu) \leq \sqrt{W_2(\mu, \nu)}$ . However, based on another fact that  $W_2(\mu, \nu) \leq [d(\mathbf{X})W_1(\mu, \nu)]^{1/2}$  where  $d(\mathbf{X})$  denotes the largest distance between two points in the compact input space  $\mathbf{X}$ , we can conclude that  $W_2(\mu, \nu)^{1/2} \leq [d(\mathbf{X})W_1(\mu, \nu)]^{1/4}$ .

Thus, to guarantee  $W_2(\mu, \nu)^{1/2} \leq W_1(\mu, \nu)$ , a sufficient condition is to show that  $[d(\mathbf{X})W_1(\mu, \nu)]^{1/4} \leq W_1(\mu, \nu)$  which is equivalent to  $d(\mathbf{X}) \leq W_1(\mu, \nu)^3$ . Thus, if  $d(\mathbf{X}) \leq W_1(\mu, \nu)^3$ , it is possible to conclude that our proposed upper bound which is based on the square root of Wasserstein-2 distance is tighter than other bounds based on Wasserstein-1 distance. In fact, for a given  $d(\mathbf{X})$ , a larger value of  $W_1(\mu, \nu)$  distance, a higher chance that the sufficient condition holds. In conclusion, there are regimes where one bound is tighter than the other.

## 2.2 Proposed methods

The upper bound in Theorem 1 is composed of three terms. Since the third term is independent of both the representation function  $f$  and the labeling function  $g$ , we can mainly focus on designing  $f$  and  $g$  to minimize the first and second terms. Following previous work [Albuquerque et al., 2019, Ben-David et al., 2007, 2010], we optimize the first term by training  $f$  together with  $g$  using a standard cross-entropy (CE) loss, such that the empirical risk on seen domains is minimized. The loss function can be written as:

$$\mathcal{L}_c(f, g) = \min_{f, g} \sum_{s=1}^S \mathbb{E}_{\mathbf{x} \sim \mu^{(s)}} [\text{CE}(h^{(s)}(\mathbf{x}), g(f(\mathbf{x})))] \quad (8)$$

where  $\text{CE}(h^{(s)}(\mathbf{x}), g(f(\mathbf{x})))$  denotes the cross entropy (CE) loss between the output of classifier and the ground-truth label of seen domain  $s$ .

The unavailability of the data distribution from unseen domain hinders the direct optimization of the second term in Eq. (6). To address this issue, we propose to use the Wasserstein-2 barycenter of the representation distributions from seen domains as a proxy for the representation distribution from the unseen domain, leading to the following loss term:

$$\mathcal{L}_{bary}(f) := \min_{\mu} \sum_{s=1}^S \frac{1}{S} W_2^2(\mu, f_{\#}\mu^{(s)}). \quad (9)$$

In contrast to previous Wasserstein distance-based method [Zhou et al., 2021a] where pairwise Wasserstein distance loss is employed, we motivate the Wasserstein barycenter loss from Eq. (6). One can easily observe that the second term in Eq. (6) has a similar form with the barycenter loss in Eq. (9). Without any extra information about the distribution of the unseen domain, we assume that the pushforward of unseen distribution  $f_{\#}\mu^{(u)}$  lies not far from the Wasserstein-2 barycenter formed by the pushforward of the seen distributions  $\{f_{\#}\mu^{(s)}\}_{s=1}^S$ , and thus can be represented by the

Wasserstein-2 barycenter term. Under such assumption, optimizing the barycenter loss will lead to the minimization of the proposed upper bound. Further, note that from the definition in Eq. 9, computing barycenter loss requires computing  $S$  Wasserstein distances in contrast to  $S(S - 1)/2$  when using pairwise Wasserstein distances. Even though the motivation of Wasserstein barycenter is somewhat heuristic, the importance of the use of Wasserstein barycenter loss is proven in our ablation study in Section 4.1.

Furthermore, to incorporate our assumption that  $f$  is manifold restricted invertible, we empirically explore two methods to enforce this constraint, i.e., reconstruction-based method and mutual information-based method.

The first method is inspired by the structure of auto-encoder, which is commonly used for dimension reduction and data denoising [Wang et al., 2016, Vincent et al., 2008]. We adopt the encoder-decoder structure and introduce reconstruction loss to approximate the invertibility constraint. More specifically, a decoder  $\psi : \mathbb{R}^{d'} \rightarrow \mathbb{R}^d$  is introduced, leading to the following loss term:

$$\min_{f, \psi} \sum_{s=1}^S \mathbb{E}_{\mathbf{x} \sim \mu^{(s)}} \|\mathbf{x} - \psi(f(\mathbf{x}))\|^2. \quad (10)$$

The other method is motivated by the manifold hypothesis and rate-distortion theory. Particularly, we propose to use mutual information (MI)  $I(\mathbf{X}^{(s)}; f(\mathbf{X}^{(s)}))$  between the input of seen domain  $s$  and its (noisy) representation as a measure of the invertibility of  $f$ . The MI quantifies the dependence between  $\mathbf{X}^{(s)}$  and  $f(\mathbf{X}^{(s)})$ , the larger the mutual information is, the more statistically dependent between the input and its representation. In other words, if  $f$  fails to achieve the invertibility, the MI term will be small due to the loss of information after representation mapping. If the representation map is exactly invertible, then the information loss after mapping is, of course, zero. This gives rise to the following term:

$$\min_f - \sum_{s=1}^S I(\mathbf{X}^{(s)}; f(\mathbf{X}^{(s)})). \quad (11)$$

From the previous analysis, to enforce the invertibility constraint while balancing the other objectives, we propose two objective functions in Eq. (12) and Eq. (13) which can be interpreted as a Lagrangian approach:

$$\arg \min_{f, g, \psi} \mathcal{L}_c(f, g) + \alpha \mathcal{L}_{bary}(f) + \beta \sum_{s=1}^S \mathbb{E}_{\mathbf{x} \sim \mu^{(s)}} \|\mathbf{x} - \psi(f(\mathbf{x}))\|^2, \quad (12)$$

and

$$\arg \min_{f, g} \mathcal{L}_c(f, g) + \alpha \mathcal{L}_{bary}(f) - \beta \sum_{s=1}^S I(\mathbf{X}^{(s)}; f(\mathbf{X}^{(s)})), \quad (13)$$

where  $\alpha, \beta > 0$  are hyperparameters.

It can be seen that the proposed upper bound is extensively incorporated by our objective functions in Eq. (12) and (13). Particularly, the first term in both objective functions aims to determine a

good classifier  $g$  together with a representation mapping  $f$  by minimizing the training error, which corresponds to the first term of the upper bound in Eq. (6). The second term in Eq. (12) and (13) minimizes the discrepancy between seen and unseen domains, contributing to a domain-invariant mapping. Motivated by the proposed upper bound, we treat the Wasserstein-2 barycenter as a proxy of the representation distribution of the unseen domain. In this way, it shares the same form with the second term in the upper bound, making it possible to minimize the discrepancy of different domains directly. Noting that though  $L_{bary}$  itself requires solving an optimization problem, we leverage fast computation methods, which is also discussed in Section 3, to directly estimate this loss without invoking the Kantorovich-Rubenstein dual characterization of Wasserstein distances [Villani, 2003, Santambrogio, 2015]. This avoids solving for a min-max type problem that is often plagued with unstable numerical dynamics. Moreover, according to the manifold invertibility assumption required in Theorem 1, we add the third term in Eq. (12) and (13).

### 3 Algorithms

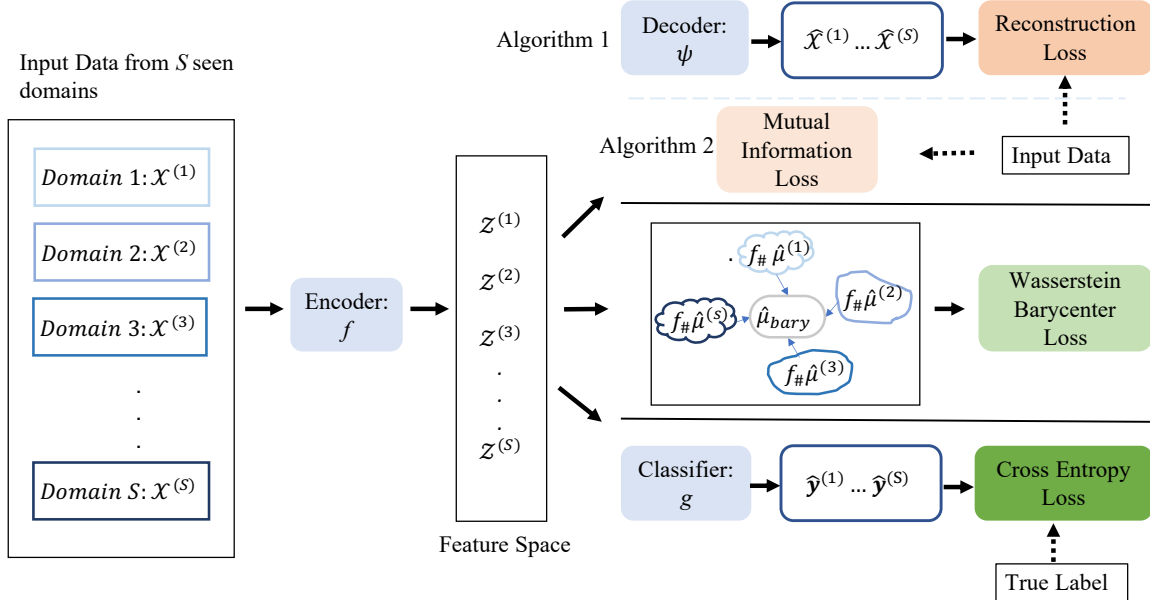


Figure 1: An overview of the proposed algorithms. On the top branch, two sub-branches refer to either choosing Algorithm 1 or Algorithm 2.

Based on the loss functions designed above, we propose algorithms for DG problem, which aim to learn domain-invariant but task-sensitive representations. Depending on how the invertibility criteria is dealt with, we design two different algorithms. Algorithm 1 adopts the auto-encoder structure to maintain the invertibility, while Algorithm 2 adds a mutual information term in the loss function for enforcing it. An overview of the proposed methods is shown in Fig.1.

Both algorithms involve calculating Wasserstein-2 barycenter and its supporting points. Here we use an off-the-shelf python package [Flamary et al., 2021] that implements a free-support Wasserstein barycenter algorithm described in [Cuturi and Doucet, 2014]. This algorithm is executed in the primal

domain and avoids the use of the dual form of Wasserstein distances, which otherwise would turn the problem into an adversarial (min-max) type setting that we want to avoid due to its instability. Given the Wasserstein barycenter estimate, the overall barycenter loss is approximated via an average Sinkhorn divergence [Feydy et al., 2019] between the seen domains and the estimated barycenter. Sinkhorn divergence is unbiased, a good proxy for the Wasserstein distance, and leverages entropic regularization [Cuturi, 2013] for computational efficiency, thereby allowing for integrating automatic differentiation with GPU computation. We adopt the implementation in [Feydy et al., 2019] to our algorithm for a fast gradient computation and denote it as  $\text{Sinkhorn}_\epsilon$ , where  $\epsilon$  is the entropic regularization term.

Algorithm 1 uses an encoder  $f$  for feature extraction and a decoder  $\psi$  for enforcing the invertibility, which are parameterized by  $\theta_e$  and  $\theta_d$ , respectively. Here we denote  $\mathcal{X}^{(s)}$  as a set of samples from domain  $s$  with empirical distribution  $\hat{\mu}^{(s)}$  and  $\mathbf{x}_i^{(s)}$  as one of its element. The corresponding label set of  $\mathcal{X}^{(s)}$  is  $\mathbf{y}^{(s)} := \{y_i^{(s)}\}$  with  $y_i^{(s)}$  is the label for sample  $\mathbf{x}_i^{(s)}$ . The extracted feature  $f_{\theta_e}(\mathbf{x}_i^{(s)})$  in set  $\mathcal{Z}^{(s)}$  is expressed as  $\mathbf{z}_i^{(s)}$  under the empirical distribution of  $f_{\#}\hat{\mu}^{(s)}$ . The decoder takes the extracted features as input and outputs the reconstructions as  $\psi_{\theta_d}(\mathbf{z}_i^{(s)})$  for domain  $s$ . The classifier  $g$ , which is parameterized by  $\theta_c$  is applied to the extracted features for label prediction.

---

**Algorithm 1** Wasserstein Barycenter Loss with Auto-Encoder (WBAE)

---

Input: Data from  $S$  seen domains, batch size  $m$ , learning rate  $\eta$ , parameters  $\alpha, \beta, \epsilon$   
 Output: Encoder  $f_{\theta_e}$ , decoder  $\psi_{\theta_d}$ , classifier  $g_{\theta_c}$

- 1: **while** Stopping criterion is not met **do**
- 2: Randomly sample a total number of  $m$  data points from  $S$  domains, where each domain has  $m^{(s)} = \frac{m}{S}$  samples, denoted as  $\mathcal{X}^{(s)} := \{\mathbf{x}_i^{(s)}\}_{i=1}^{m^{(s)}}$  and  $\mathbf{y}^{(s)} := \{y_i^{(s)}\}_{i=1}^{m^{(s)}}$ , the empirical distribution for the data is denoted as  $\hat{\mu}^{(s)}$
- 3: **for**  $s = 1 : S$  and  $i = 1 : m^{(s)}$  **do**
- 4:    $\mathbf{z}_i^{(s)} \leftarrow f_{\theta_e}(\mathbf{x}_i^{(s)})$  with set  $\mathcal{Z}^{(s)}$  under distribution  $f_{\#}\hat{\mu}^{(s)}$
- 5: **end for**
- 6: Calculate the Wasserstein barycenter  $\hat{\mu}_{bary}$  of  $\{f_{\#}\hat{\mu}^{(s)}\}_{s=1}^S$  and its supporting points with  $f_{\theta_e}$  detached from automatic backpropagation
- 7: Compute the Wasserstein barycenter loss as  $\mathcal{L}_{wb} = \frac{1}{S} \sum_{s=1}^S \text{Sinkhorn}_\epsilon(\hat{\mu}_{bary}, f_{\#}\hat{\mu}^{(s)})$
- 8: Calculate the classification loss as  $\mathcal{L}_c = -\frac{1}{m} \sum_{s=1}^S \sum_{i=1}^{m^{(s)}} y_i^{(s)} \log p(g_{\theta_c}(f_{\theta_e}(\mathbf{x}_i^{(s)})))$
- 9: Calculate the reconstruction loss as  $\mathcal{L}_r = \frac{1}{m} \sum_{s=1}^S \sum_{i=1}^{m^{(s)}} \|\mathbf{x}_i^{(s)} - \psi_{\theta_d}(\mathbf{z}_i^{(s)})\|_2^2$
- 10:  $\theta_c = \theta_c - \eta \nabla_{\theta_c} \mathcal{L}_c$ ,    $\theta_d = \theta_d - \eta \nabla_{\theta_d} \mathcal{L}_r$
- 11:  $\mathcal{L} = \mathcal{L}_c + \alpha \mathcal{L}_{wb} + \beta \mathcal{L}_r$
- 12:  $\theta_e = \theta_e - \eta \nabla_{\theta_e} \mathcal{L}$
- 13: **end while**

---

As a surrogate of the decoder  $\psi_{\theta_d}$ , we consider maximizing the mutual information between the input data and the extracted feature as an objective to obligate the invertibility, which motivates Algorithm 2. Since mutual information is intractable when the distribution is unknown, we adopt

the Mutual Information Gradient Estimation (MIGE) [Wen et al., 2020] framework to estimate the gradient of mutual information between the distribution of the input data and the extracted feature. Moreover, to avoid the mutual information going to infinity, we add a small noise to the extracted feature.

---

**Algorithm 2** Wasserstein Barycenter Loss with Mutual Information (WBMI)

---

Input: Data from  $S$  seen domains, batch size  $m$ , learning rate  $\eta$ , parameters  $\alpha, \beta, \delta, \epsilon$   
 Output: Encoder  $f_{\theta_e}$ , classifier  $g_{\theta_c}$

- 1: **while** Stopping criterion is not met **do**
- 2: Randomly sample a total number of  $m$  data points from  $S$  domains, where each domain has  $m^{(s)} = \frac{m}{S}$  samples, denoted as  $\mathcal{X}^{(s)} := \{\mathbf{x}_i^{(s)}\}_{i=1}^{m^{(s)}}$  and  $\mathbf{y}^{(s)} := \{y_i^{(s)}\}_{i=1}^{m^{(s)}}$ , the empirical distribution for the data is denoted as  $\hat{\mu}^{(s)}$
- 3: **for**  $s = 1 : S$  and  $i = 1 : m^{(s)}$  **do**
- 4:    $\mathbf{z}_i^{(s)} \leftarrow f_{\theta_e}(\mathbf{x}_i^{(s)})$  with set  $\mathcal{Z}^{(s)}$  under distribution  $f_{\#}\hat{\mu}^{(s)}$
- 5:    $\mathcal{Z}_{noise}^{(s)} \leftarrow \mathcal{Z}^{(s)} + \delta\mathcal{N}(0, 1)$
- 6: **end for**
- 7: Calculate the Wasserstein barycenter  $\hat{\mu}_{bary}$  of  $\{f_{\#}\hat{\mu}^{(s)}\}_{s=1}^S$  and its supporting points with  $f_{\theta_e}$  detached from automatic backpropagation
- 8: Compute the Wasserstein barycenter loss as  $\mathcal{L}_{wb} = \frac{1}{S} \sum_{s=1}^S \text{Sinkhorn}_{\epsilon}(\hat{\mu}_{bary}, f_{\#}\hat{\mu}^{(s)})$
- 9: Calculate the classification loss as  $\mathcal{L}_c = -\frac{1}{m} \sum_{s=1}^S \sum_{i=1}^{m^{(s)}} y_i^{(s)} \log p(g_{\theta_c}(f_{\theta_e}(\mathbf{x}_i^{(s)})))$
- 10: Estimate the gradient of mutual information between the empirical distribution of  $\{\mathcal{X}^{(s)}\}_{s=1}^S$  and  $\{\mathcal{Z}_{noise}^{(s)}\}_{s=1}^S$  via MIGE, denoted as  $\nabla_{\theta_e} \mathcal{L}_i$
- 11:  $\theta_c = \theta_c - \eta \nabla_{\theta_c} \mathcal{L}_c$
- 12:  $\theta_e = \theta_e - \eta(\alpha \nabla_{\theta_e} \mathcal{L}_{wb} - \beta \nabla_{\theta_e} \mathcal{L}_i)$
- 13: **end while**

---

## 4 Experiments and Results

**Datasets:** To evaluate proposed methods, we conduct experiments on two commonly used object recognition datasets for DG: Office-Caltech [Gong et al., 2012] and Office-Home [Venkateswara et al., 2017] dataset.

- **Office-Caltech:** Office-Caltech dataset consists of 2533 images from 4 different domains: Amazon (A), Webcam (W), Caltech-256 (C), and DSLR (D), where a total of 10 classes are shared by all domains. Instead of images, we use the 4096 dimensional DeCAF<sub>6</sub> features [Donahue et al., 2014] as input.
- **Office-Home:** Office-Home dataset is a larger dataset with 15,500 images from 4 different domains: Artistic images (A), Clip Art (C), Product images (P), and Real-World (R). Each domain has 65 common object categories. We adopt the publicly-available deep features [Wang et al.] extracted by the fine-tuned ResNet-50 model for each domain.

**Methods Compared:** We compare our methods against the following algorithms.

- **ERM**: The Empirical Risk Minimization method serves as a baseline. We train a feature extractor and a classifier on the data from all seen domains without performing any DG techniques. The feature extractor has three fully connected (FC) layers with ReLU as the activation function. For the Office-Caltech dataset, the output dimension of three FC layers is 1024, 800, and 200, while for Office-Home is 1024, 512, and 100. The classifier is a one linear layer model with the output dimension as the number of classes. The feature extractor and classifier are trained together using cross-entropy loss with a batch size of 64.
- **MLDG** [Li et al., 2018a]: The meta-learning domain generalization approach provides a training procedure that fits different models. It divides multiple seen domains into meta-train and meta-test domains to mimic domain shift and conducts optimization to improve model performance over meta-train and meta-test data. We use the same feature extractor and classifier as in the ERM method for both datasets and the implementation in [Gulrajani and Lopez-Paz, 2020] for meta-learning optimization. The batch size is set to 150 with samples equally picked from each seen domain for Office-Caltech dataset and doubled for Office-Home dataset.
- **DANN** [Ganin et al., 2016]: The domain adversarial neural network is a DA method which trains a domain-invariant feature extractor together with a domain discriminator via adversarial training process. It is widely used in DA problems and the idea of learning a domain-invariant representation motivated some of the adversarial approaches in DG. We reference a recent GitHub project <sup>1</sup> for the gradient reversal layer implementation and [Gulrajani and Lopez-Paz, 2020] for the training process. We use the same feature extractor and classifier as in the ERM method for both datasets, but with an additional linear layer that serves as the adversarial domain discriminator. The batch size is set to be 64 for Office-Caltech dataset and 160 for Office-Home dataset.
- **MMD-AAE** [Li et al., 2018b]: The maximum mean discrepancy (MMD)-adversarial autoencoder aligns the representation distributions from different domains via minimizing their MMD and matches the learned representation distribution to a prior distribution in an adversarial manner. Since the code is not released from the author, we reference [Gulrajani and Lopez-Paz, 2020] for their MMD loss calculation and implement the other part of the algorithm by ourselves. Following the original MMD-AAE paper, we choose the prior distribution as Laplace distribution for adversarial training. For MMD estimation, a mixture kernel is used via averaging the RBF kernels with the bandwidth  $\sigma = 1, 5, 10$ , as also suggested in the original paper [Li et al., 2018b]. We use the same feature extractor and classifier as in the ERM method for both datasets, but with an additional linear layer that serves as the adversarial domain discriminator. The batch size is set to be the same as that for MLDG.

**Training Procedure:** We follow the leave-one-domain-out protocol in [Dou et al., 2019] to conduct DG tasks. Data from each domain is randomly split into training and validation sets in the proportion

---

<sup>1</sup>[https://github.com/fungtion/DANN\\_py3](https://github.com/fungtion/DANN_py3)

80% and 20% respectively. During training, we aggregated the training/validation from each seen domain to form the overall training/validation set. For tuning hyper-parameters, we perform a grid search over a range [0.01,10] with a  $\log_{10}$  scale and choose parameters that produce the lowest averaged validation loss over all DG tasks. After fixing the hyper-parameters, we re-train the model and select the one with the lowest validation loss to generate the final classification accuracy on the test domain data. This hyper-parameter tuning and model selection strategy is applied to all models that we evaluate. Models are trained for 300 epochs using the Adam optimizer [Kingma and Ba, 2015] with the learning rate of  $5 \times 10^{-5}$  for Office-Caltech dataset and  $5 \times 10^{-4}$  for the Office-Home dataset. We use Nvidia-tesla p100 16 GB GPU for computation and one round of training (300 epochs) will take half an hour for the proposed methods. The above procedure is repeated five times for each model and the average accuracy and standard deviation values are reported.

- **Experiments on Office-Caltech dataset:** The model structure of our proposed algorithms is kept consistent with that used in the comparison methods. In particular, we use the same three fully connected layer model and one linear layer model for the encoder (feature extractor) and classifier, respectively. The decoder in Algorithm 1 shares the same structure as the encoder but in reverse order. The batch size  $m$  is set to 150. The values of  $\epsilon$  for the Sinkhorn loss and  $\delta$  for Gaussian noise are empirically chosen without tuning and fixed at 0.5 and 0.1, respectively, for all tasks. The  $(\alpha, \beta)$  pair is set to (0.01, 10) for Algorithm 1 and (0.1, 0.01) for Algorithm 2.
- **Experiments on Office-Home dataset:** For the proposed methods, we double the batch size to 300 as in MLDG. The  $(\alpha, \beta)$  pair is set to (0.01, 1) for Algorithm 1 and (0.1, 1) for Algorithm 2. The model structure used for our proposed methods is kept consistent with that used in the comparison methods. All the other settings are the same as that for the Office-Caltech dataset.

**Results:** Results for the Office-Caltech dataset are shown in Table 1. Both the proposed algorithms have very similar performance with only modest improvements over all the comparison methods. The comparable performance of all methods can be attributed to the small size of the dataset and the limited diversity between domains. However, when we examine results for the larger and more challenging Office-Home dataset, our methods outperform the comparison methods which include DA method, meta-learning based method, and adversarial DG method, in all four tasks as shown in Table 2. Specifically, the WBAE outperforms all the comparison methods by at least 4.2% on average and by 3.9%, 5.4%, and 4.3% and 3.1% on each task. A larger performance improvement is observed with our WBMI method, boosting the classification accuracy by at least 6.3 percentage points on average compared to all the comparison methods and by 6.5%, 8.0%, and 5.5% and 4.9% on each task.

## 4.1 Ablation Study

To study the impact of different components of the total loss function, we conduct a full ablation study for the WBAE method and a partial one for WBMI method on both datasets. In particular, we consider the following variants of our method: (1) WBAE without Wasserstein barycenter loss, denoted as WBAE-L<sub>wb</sub>; (2) WBAE without reconstruction loss, denoted as WBAE-L<sub>r</sub>, this variant can also

Table 1: Performance on Office-Caltech Dataset

Unseen	ERM	DANN	MMD-AAE	MLDG	WBAE	WBMI
A	$90.8 \pm 0.9$	$91.1 \pm 0.4$	$90.9 \pm 0.6$	$90.2 \pm 0.6$	$91.3 \pm 0.5$	<b><math>91.9 \pm 0.7</math></b>
C	$81.8 \pm 1.8$	$83.2 \pm 1.1$	$82.5 \pm 1.5$	$82.8 \pm 0.9$	$84.1 \pm 1.0$	<b><math>84.4 \pm 0.4</math></b>
D	$96.4 \pm 1.0$	$96.7 \pm 2.2$	$97.6 \pm 0.8$	$98.3 \pm 1.1$	<b><math>98.5 \pm 0.3</math></b>	$98.1 \pm 1.2$
W	$88.4 \pm 1.5$	$90.4 \pm 1.8$	$93.7 \pm 1.4$	<b><math>93.8 \pm 1.5</math></b>	$93.4 \pm 2.0$	$92.9 \pm 1.4$
Average	$89.4 \pm 1.4$	$90.4 \pm 1.5$	$91.2 \pm 1.1$	$91.3 \pm 1.1$	$91.8 \pm 1.2$	<b><math>91.8 \pm 1.0</math></b>

Table 2: Performance on Office-Home Dataset

Unseen	ERM	DANN	MMD-AAE	MLDG	WBAE	WBMI
A	$65.7 \pm 0.3$	$67.0 \pm 0.5$	$66.4 \pm 0.8$	$67.5 \pm 0.7$	$71.4 \pm 0.4$	<b><math>74.0 \pm 0.5</math></b>
C	$62.1 \pm 1.6$	$63.1 \pm 0.5$	$62.7 \pm 0.8$	$62.9 \pm 1.1$	$68.5 \pm 0.3$	<b><math>71.1 \pm 0.5</math></b>
P	$79.8 \pm 1.3$	$80.1 \pm 0.8$	$80.4 \pm 1.1$	$80.3 \pm 0.4$	$84.7 \pm 0.7$	<b><math>85.9 \pm 0.3</math></b>
R	$81.4 \pm 0.3$	$82.0 \pm 1.1$	$82.0 \pm 0.4$	$82.1 \pm 0.3$	$85.2 \pm 0.2$	<b><math>87.0 \pm 0.3</math></b>
Average	$72.2 \pm 1.1$	$73.0 \pm 0.8$	$72.9 \pm 0.8$	$73.2 \pm 0.7$	$77.4 \pm 0.4$	<b><math>79.5 \pm 0.4</math></b>

Table 3: Office-Caltech Dataset

Unseen	WBAE-L <sub>wb</sub>	WBAE-L <sub>r</sub> WBMI-L <sub>i</sub>	WBAE	WBMI
A	$90.5 \pm 0.7$	$91.3 \pm 0.7$	$91.3 \pm 0.5$	<b><math>91.9 \pm 0.7</math></b>
C	$82.2 \pm 0.7$	$83.8 \pm 0.9$	$84.1 \pm 1.0$	<b><math>84.4 \pm 0.4</math></b>
D	$98.1 \pm 0.9$	<b><math>98.7 \pm 0.6</math></b>	$98.5 \pm 0.3$	$98.1 \pm 1.2$
W	$92.5 \pm 1.6$	$92.9 \pm 1.7$	<b><math>93.4 \pm 2.0</math></b>	$92.9 \pm 1.4$
Average	$90.9 \pm 1.0$	$91.7 \pm 1.1$	$91.8 \pm 1.2$	<b><math>91.8 \pm 1.0</math></b>

Table 4: Office-Home Dataset

Unseen	WBAE-L <sub>wb</sub>	WBAE-L <sub>r</sub> WBMI-L <sub>i</sub>	WBAE	WBMI
A	$66.8 \pm 0.8$	$71.4 \pm 0.7$	$71.4 \pm 0.4$	<b><math>74.0 \pm 0.5</math></b>
C	$63.4 \pm 0.6$	$68.5 \pm 0.4$	$68.5 \pm 0.3$	<b><math>71.1 \pm 0.5</math></b>
P	$80.2 \pm 0.6$	$84.6 \pm 0.7$	$84.7 \pm 0.7$	<b><math>85.9 \pm 0.3</math></b>
R	$82.2 \pm 0.9$	$85.2 \pm 0.3$	$85.2 \pm 0.2$	<b><math>87.0 \pm 0.3</math></b>
Average	$73.2 \pm 0.7$	$77.4 \pm 0.6$	$77.4 \pm 0.4$	<b><math>79.5 \pm 0.4</math></b>

be viewed as WBMI method without mutual information loss, so we also denote it as WBMI-L<sub>i</sub>; (3) original WBAE method with all the loss components, denoted as WBAE; (4) original WBMI method with all the loss components denotes as WBMI. During the experiment, we remove the decoder part for WBAE-L<sub>r</sub> and keep all the other model architectures, parameter tuning and validation process the same as above.

From Table 3 and Table 4, we find that removing L<sub>r</sub> from WBAE model leads to a decrease in the accuracy of around 1.5% for Office-Caltech dataset and 1% for Office-Home dataset. The performance deterioration can be more clearly observed when omitting L<sub>wb</sub> for WBAE model, leading to a drop of around 2.3% for Office-Caltech dataset and 5.2% for Office-Home dataset. More interestingly, we observe a 2.1% improvement in accuracy when replacing the reconstruction loss L<sub>r</sub> in WBAE with the mutual information loss when comparing WBAE-L<sub>r</sub>/WBMI-L<sub>i</sub> with the full WBAE and WBMI.

This ablation study demonstrates the importance of the Wasserstein barycenter loss and also stresses the key role of the invertibility of the representation mapping. This is reflected in the performance of WBMI in achieving the best results overall, which also indicates that the use of auto-encoder may be more limited than using mutual information as a criteria. On the other hand, the estimation of the

gradient for mutual information may not be accurate in higher dimensions, which is one limitation of the proposed WBMI method.

## 5 Conclusions and Future Work

We revisited the theory and methods for DG and provided a new upper bound for the risk of unseen domain. Our analysis could be potentially tightened towards understanding minimal regularity conditions on the distribution and the loss functions that can yield better bounds or a family of bounds adapted to different situations. In terms of algorithms and numerical implementation, we note that our methods, although numerically stable and have better accuracy compared to adversarial and other related approaches, can be computationally expensive. This cost is primarily driven by the need to reliably estimate the Wasserstein-2 barycenter, which is known to require a large number of samples in high dimensions [Korotin et al., 2021]. To alleviate this, one can employ the recently proposed large scale barycenter and mapping estimators [Fan et al., 2020]. It is to be noted that using adversarial approaches also suffer from the same sample complexity issues in order to reliably estimate the domain discrepancy in the representation space. The gradient estimation of mutual information is also known to degrade in higher dimensions and one can leverage some recent advances made to alleviate this issue [Belghazi et al., 2018, Wen et al., 2020].

## References

H. Ajakan, P. Germain, H. Larochelle, F. Laviolette, and M. Marchand. Domain-adversarial neural networks. *arXiv preprint arXiv:1412.4446*, 2014.

I. Albuquerque, J. Monteiro, M. Darvishi, T. H. Falk, and I. Mitliagkas. Generalizing to unseen domains via distribution matching. *arXiv preprint arXiv:1911.00804*, 2019.

T. Batu, L. Fortnow, R. Rubinfeld, W. D. Smith, and P. White. Testing that distributions are close. In *Proceedings 41st Annual Symposium on Foundations of Computer Science*, pages 259–269. IEEE, 2000.

M. I. Belghazi, A. Baratin, S. Rajeshwar, S. Ozair, Y. Bengio, A. Courville, and D. Hjelm. Mutual information neural estimation. In *International Conference on Machine Learning*, pages 531–540. PMLR, 2018.

S. Ben-David, J. Blitzer, K. Crammer, F. Pereira, et al. Analysis of representations for domain adaptation. *Advances in neural information processing systems*, 19:137, 2007.

S. Ben-David, J. Blitzer, K. Crammer, A. Kulesza, F. Pereira, and J. W. Vaughan. A theory of learning from different domains. *Machine learning*, 79(1):151–175, 2010.

D. Berend, P. Harremoës, and A. Kontorovich. Minimum kl-divergence on complements of  $l_1$  balls. *IEEE Transactions on Information Theory*, 60(6):3172–3177, 2014. doi: 10.1109/TIT.2014.2301446.

G. Blanchard, G. Lee, and C. Scott. Generalizing from several related classification tasks to a new unlabeled sample. *Advances in neural information processing systems*, 24:2178–2186, 2011.

I. Csiszár and J. Körner. *Information theory: coding theorems for discrete memoryless systems*. Cambridge University Press, 2011.

Y. Cui, Y. Xu, and D. Wu. Eeg-based driver drowsiness estimation using feature weighted episodic training. *IEEE transactions on neural systems and rehabilitation engineering*, 27(11):2263–2273, 2019.

M. Cuturi. Sinkhorn distances: Lightspeed computation of optimal transport. *Advances in neural information processing systems*, 26:2292–2300, 2013.

M. Cuturi and A. Doucet. Fast computation of wasserstein barycenters. In *International conference on machine learning*, pages 685–693. PMLR, 2014.

J. Donahue, Y. Jia, O. Vinyals, J. Hoffman, N. Zhang, E. Tzeng, and T. Darrell. Decaf: A deep convolutional activation feature for generic visual recognition. In *International conference on machine learning*, pages 647–655. PMLR, 2014.

Q. Dou, D. C. Castro, K. Kamnitsas, and B. Glocker. Domain generalization via model-agnostic learning of semantic features. *arXiv preprint arXiv:1910.13580*, 2019.

J. Fan, A. Taghvaei, and Y. Chen. Scalable computations of wasserstein barycenter via input convex neural networks. *arXiv preprint arXiv:2007.04462*, 2020.

J. Feydy, T. Séjourné, F.-X. Vialard, S.-i. Amari, A. Trouve, and G. Peyré. Interpolating between optimal transport and mmd using sinkhorn divergences. In *The 22nd International Conference on Artificial Intelligence and Statistics*, pages 2681–2690, 2019.

R. Flamary, N. Courty, A. Gramfort, M. Z. Alaya, A. Boisbunon, S. Chambon, L. Chapel, A. Corenflos, K. Fatras, N. Fournier, L. Gautheron, N. T. Gayraud, H. Janati, A. Rakotomamonjy, I. Redko, A. Rolet, A. Schutz, V. Seguy, D. J. Sutherland, R. Tavenard, A. Tong, and T. Vayer. Pot: Python optimal transport. *Journal of Machine Learning Research*, 22(78):1–8, 2021. URL <http://jmlr.org/papers/v22/20-451.html>.

Y. Ganin, E. Ustinova, H. Ajakan, P. Germain, H. Larochelle, F. Laviolette, M. Marchand, and V. Lempitsky. Domain-adversarial training of neural networks. *The journal of machine learning research*, 17(1):2096–2030, 2016.

M. Ghifary, W. B. Kleijn, M. Zhang, and D. Balduzzi. Domain generalization for object recognition with multi-task autoencoders. In *Proceedings of the IEEE international conference on computer vision*, pages 2551–2559, 2015.

B. Gong, Y. Shi, F. Sha, and K. Grauman. Geodesic flow kernel for unsupervised domain adaptation. In *2012 IEEE conference on computer vision and pattern recognition*, pages 2066–2073. IEEE, 2012.

I. Goodfellow, J. Pouget-Abadie, M. Mirza, B. Xu, D. Warde-Farley, S. Ozair, A. Courville, and Y. Bengio. Generative adversarial nets. *Advances in neural information processing systems*, 27, 2014.

I. Gulrajani and D. Lopez-Paz. In search of lost domain generalization. *arXiv preprint arXiv:2007.01434*, 2020.

D. Kifer, S. Ben-David, and J. Gehrke. Detecting change in data streams. In *VLDB*, volume 4, pages 180–191. Toronto, Canada, 2004.

D. P. Kingma and J. Ba. Adam: A method for stochastic optimization. In Y. Bengio and Y. LeCun, editors, *3rd International Conference on Learning Representations, ICLR 2015, San Diego, CA, USA, May 7-9, 2015, Conference Track Proceedings*, 2015. URL <http://arxiv.org/abs/1412.6980>.

A. Korotin, L. Li, J. Solomon, and E. Burnaev. Continuous wasserstein-2 barycenter estimation without minimax optimization. *arXiv preprint arXiv:2102.01752*, 2021.

N. Lei, D. An, Y. Guo, K. Su, S. Liu, Z. Luo, S.-T. Yau, and X. Gu. A geometric understanding of deep learning. *Engineering*, 6(3):361–374, 2020. ISSN 2095-8099. doi: <https://doi.org/10.1016/j.eng.2019.09.010>. URL <https://www.sciencedirect.com/science/article/pii/S2095809919302279>.

D. Li, Y. Yang, Y.-Z. Song, and T. Hospedales. Learning to generalize: Meta-learning for domain generalization. In *Proceedings of the AAAI Conference on Artificial Intelligence*, volume 32, 2018a.

H. Li, S. J. Pan, S. Wang, and A. C. Kot. Domain generalization with adversarial feature learning. In *Proceedings of the IEEE Conference on Computer Vision and Pattern Recognition*, pages 5400–5409, 2018b.

B. Lyu, T. Pham, G. Blaney, Z. Haga, A. Sassaroli, S. Fantini, and S. Aeron. Domain adaptation for robust workload level alignment between sessions and subjects using fNIRS. *Journal of Biomedical Optics*, 26(2):1 – 21, 2021. doi: 10.1117/1.JBO.26.2.022908. URL <https://doi.org/10.1117/1.JBO.26.2.022908>.

G. Peyré and M. Cuturi. Computational optimal transport. *Foundations and Trends in Machine Learning*, 11 (5-6):355–602, 2019.

Y. Polyanskiy and Y. Wu. Wasserstein continuity of entropy and outer bounds for interference channels. *IEEE Transactions on Information Theory*, 62(7):3992–4002, 2016.

I. Redko, A. Habrard, and M. Sebban. Theoretical analysis of domain adaptation with optimal transport. In *Joint European Conference on Machine Learning and Knowledge Discovery in Databases*, pages 737–753. Springer, 2017.

I. Redko, E. Morvant, A. Habrard, M. Sebban, and Y. Bennani. A survey on domain adaptation theory: learning bounds and theoretical guarantees. *arXiv e-prints*, pages arXiv–2004, 2020.

F. Santambrogio. *Optimal Transport for Applied Mathematicians: Calculus of Variations, PDEs and Modeling*. Springer, 2015.

J. Shen, Y. Qu, W. Zhang, and Y. Yu. Wasserstein distance guided representation learning for domain adaptation. In *Proceedings of the AAAI Conference on Artificial Intelligence*, volume 32, 2018.

A. van den Oord, Y. Li, and O. Vinyals. Representation learning with contrastive predictive coding. *CoRR*, abs/1807.03748, 2018. URL <http://arxiv.org/abs/1807.03748>.

H. Venkateswara, J. Eusebio, S. Chakraborty, and S. Panchanathan. Deep hashing network for unsupervised domain adaptation. In *Proceedings of the IEEE conference on computer vision and pattern recognition*, pages 5018–5027, 2017.

C. Villani. *Topics in optimal transportation*. Number 58. American Mathematical Soc., 2003.

P. Vincent, H. Larochelle, Y. Bengio, and P.-A. Manzagol. Extracting and composing robust features with denoising autoencoders. In *Proceedings of the 25th international conference on Machine learning*, pages 1096–1103, 2008.

J. Wang, C. Lan, C. Liu, Y. Ouyang, and T. Qin. Generalizing to unseen domains: A survey on domain generalization. *arXiv e-prints*, pages arXiv–2103, 2021.

J. Wang et al. Everything about transfer learning and domain adaption. <http://transferlearning.xyz>.

Y. Wang, H. Yao, and S. Zhao. Auto-encoder based dimensionality reduction. *Neurocomputing*, 184: 232–242, 2016.

L. Wen, Y. Zhou, L. He, M. Zhou, and Z. Xu. Mutual information gradient estimation for representation learning. *arXiv preprint arXiv:2005.01123*, 2020.

H. Zhao, S. Zhang, G. Wu, G. J. Gordon, et al. Multiple source domain adaptation with adversarial learning. 2018.

H. Zhao, R. T. Des Combes, K. Zhang, and G. Gordon. On learning invariant representations for domain adaptation. In *International Conference on Machine Learning*, pages 7523–7532. PMLR, 2019.

F. Zhou, Z. Jiang, C. Shui, B. Wang, and B. Chaib-draa. Domain generalization with optimal transport and metric learning. *arXiv preprint arXiv:2007.10573*, 2020.

F. Zhou, Z. Jiang, C. Shui, B. Wang, and B. Chaib-draa. Domain generalization via optimal transport with metric similarity learning. *Neurocomputing*, 456:469–480, 2021a. ISSN 0925-2312. doi: <https://doi.org/10.1016/j.neucom.2020.09.091>. URL <https://www.sciencedirect.com/science/article/pii/S0925231221002009>.

K. Zhou, Z. Liu, Y. Qiao, T. Xiang, and C. C. Loy. Domain generalization: A survey. *arXiv preprint arXiv:2103.02503*, 2021b.

## A Appendix

### A.1 Discussion about the shortcomings in the proposed upper bound in [Ben-David et al., 2007]

First, recall that a *domain*  $v$  is a triple  $(\mu^{(v)}, f^{(v)}, g^{(v)})$  consisting of a distribution  $\mu^{(v)}$  on the inputs  $\mathbf{x} \in \mathbb{R}^d$ , a representation function that maps an input  $\mathbf{x}$  from input space to its representation  $\mathbf{z}$  in the representation space  $f^{(v)} : \mathbb{R}^d \rightarrow \mathbb{R}^{d'}$ , and a stochastic labeling function  $g^{(v)} : \mathbb{R}^{d'} \rightarrow \mathcal{Y}$  mapping the representation space to label space  $\mathcal{Y}$ .

We denote the unseen domain by  $(\mu^{(u)}, f^{(u)}, g^{(u)})$  and the seen domain by  $(\mu^{(s)}, f^{(s)}, g^{(s)})$ . Let  $\mathcal{F} = \{f | f : \mathbb{R}^d \rightarrow \mathbb{R}^{d'}\}$  be a set of *representation functions*,  $\mathcal{G} = \{g | g : \mathbb{R}^{d'} \rightarrow \mathcal{Y}\}$  a set of stochastic *labeling functions*. Here label space  $\mathcal{Y}$  is considered as binary. A *hypothesis*  $h : \mathbb{R}^d \rightarrow \mathcal{Y}$  obtained by composing each  $g \in \mathcal{G}$  with each  $f \in \mathcal{F}$ , i.e.,  $h = g \circ f$ . Next, we rewrite Theorem 1 in [Ben-David et al., 2007] using our notations.

**Theorem 2.** [Ben-David et al., 2007] *Let  $f$  be a fixed representation function from input space to representation space and  $\mathcal{G}$  be a hypothesis space of VC-dimension  $k$ . If a random labeled sample of size  $m$  is generated by applying  $f$  to i.i.d. samples of seen domain, then with probability at least  $1 - \delta$  for every  $g \in \mathcal{G}$ :*

$$R^{(u)}(g) \leq R^{(s)}(g) + d_{\mathcal{H}}(f_{\#}\mu^{(u)}, f_{\#}\mu^{(s)}) + \lambda \quad (14)$$

$$\leq \hat{R}^{(s)}(g) + \sqrt{\frac{4}{m} \left( k \log \frac{2em}{k} + \log \frac{4}{\delta} \right)} + d_{\mathcal{H}}(f_{\#}\mu^{(u)}, f_{\#}\mu^{(s)}) + \lambda \quad (15)$$

where  $e$  is the base of the natural logarithm,  $d_{\mathcal{H}}$  is  $\mathcal{H}$ -divergence (please see Definition 1 in [Ben-David et al., 2010], Definition 2.1 in [Zhao et al., 2019] or Definition 1 in [Kifer et al., 2004]),  $R^{(u)}(g) = \mathbb{E}_{\mathbf{z} \sim f_{\#}\mu^{(u)}} |g(\mathbf{z}) - g^{(u)}(\mathbf{z})|$  denotes the risk on unseen domain,  $R^{(s)}(g) = \mathbb{E}_{\mathbf{z} \sim f_{\#}\mu^{(s)}} |g(\mathbf{z}) - g^{(s)}(\mathbf{z})|$  and  $\hat{R}^{(s)}(g)$  denote the risk on seen domain and its empirical estimate, respectively, and

$$\lambda = \inf_{g \in \mathcal{G}} (R^{(s)}(g) + R^{(u)}(g)) \quad (16)$$

is the combined risk.

Though the bound in Theorem 1 of [Ben-David et al., 2007] was originally constructed for domain adaptation problem, it has profound influences on the DG problem and extensive applications in recent DG work, as mentioned earlier in Section 1. To highlight the differences between our work and previous theoretical bounds (the bound in Theorem 1 of [Ben-David et al., 2007] and Theorem 4.1 of [Zhao et al., 2019]), a thorough comparison is made below:

- First, Ben-David et al. [2007] define the risk induced by labeling function  $g$  from the representation space to the label space based on the disagreement between  $g$  and the optimal labeling function  $g^{(u)}$ :

$$R^{(u)}(g) = \mathbb{E}_{\mathbf{z} \sim f_{\#}\mu^{(u)}} |g(\mathbf{z}) - g^{(u)}(\mathbf{z})|. \quad (17)$$

On the other hand, we define the risk induced by using a hypothesis  $h$  from input space to label space by the disagreement between  $h$  and the optimal hypothesis  $h^{(u)}$  via a loss function  $\ell(\cdot, \cdot)$ :

$$R^{(u)}(h) = \mathbb{E}_{\mathbf{x} \sim \mu^{(u)}} [\ell(h(\mathbf{x}), h^{(u)}(\mathbf{x}))]. \quad (18)$$

Since the empirical risk measures the probability of misclassification of a hypothesis that maps from the input space to the label space, minimizing  $R^{(u)}(g)$  does not guarantee to minimize the empirical risk. Particularly, if the representation function  $f$  is invertible i.e., there is a one-to-one mapping between  $\mathbf{x}$  and  $\mathbf{z}$ , and the loss function  $\ell(a, b) = |a - b|$ , then it is possible to verify that  $R^{(u)}(g) = R^{(u)}(h)$ . In general, the representation map might not be invertible. For example, let consider a representation function  $f$  that maps  $f(\mathbf{x}_1) = f(\mathbf{x}_2) = \mathbf{z}$ ,  $\mathbf{x}_1 \neq \mathbf{x}_2$ , with the corresponding labels are  $y_1 = 0$  and  $y_2 = 1$ . In this case, the risk defined in (17) will introduce a larger error than the risk introduced in (18) since  $g(\mathbf{z})$  can not be mapped to both "0" and "1". That said, the risk defined in (18) is more precise to describe the empirical risk. In addition, the risk defined in (17) is only a special case of (18) when the representation map  $f$  is invertible and the loss function satisfies  $\ell(a, b) = |a - b|$ .

- Second, for a given hypothesis space, the ideal joint hypothesis is defined as the hypothesis which globally minimizes the combined error from seen and unseen domains [Ben-David et al., 2007, 2010]. In other words, this hypothesis should work well on both domains. The error induced by using this ideal joint hypothesis is called *combined risk*:

$$\lambda = \inf_{g \in \mathcal{G}} (R^{(s)}(g) + R^{(u)}(g)).$$

Note that the labeling function is a mapping from the representation space to the label space, therefore the ideal labeling function depends implicitly on the representation function  $f$ . Simply ignoring this fact and treat  $\lambda$  as a constant may loosen the upper bound. On the contrary, our goal is to construct an upper bound with the *combined risk* term  $\sigma^{(u,s)}$  independent of both the representation function and the labeling function, which can be seen from Lemma 1 and Theorem 1.

Finally, it is worth comparing our upper bound with the bound in Theorem 4.1 of [Zhao et al., 2019] which also has the *combined risk* term free of the choice of the hypothesis class. However, noting that the result in Theorem 4.1 of [Zhao et al., 2019] does not consider any representation function  $f$  i.e., their labeling function directly maps from the input space to the label space while our hypothesis is composed by a representation function from input space to representation space followed by a labeling function from representation space to label space. Since it is possible to pick a representation function  $f$  that maps any input to itself i.e.,  $f(\mathbf{x}) = \mathbf{x}$  which leads to  $h = g \circ f = g$ , the bound in [Zhao et al., 2019] can be viewed as a special case of our proposed upper bound in Lemma 1.

## A.2 Proof of Lemma 1

First, we want to note that our approach for constructing the upper bound in Lemma 1 is motivated by the proof of Theorem 1 in [Ben-David et al., 2010]. Next, to make the dependence on the hypothesis, input distribution, and the true representation and labeling functions transparent, we use inner product notation  $\langle \cdot, \cdot \rangle$  to write expectations. Specifically,

$$R^{(v)}(h) := \mathbb{E}_{\mathbf{x} \sim \mu^{(v)}} [\ell(h(\mathbf{x}), h^{(v)}(\mathbf{x}))] = \langle \ell(h, h^{(v)}), \mu^{(v)} \rangle. \quad (19)$$

From the definition of risk,

$$\begin{aligned} R^{(u)}(h) &= \langle \ell(h, h^{(u)}), \mu^{(u)} \rangle = \langle \ell(h, h^{(s)}), \mu^{(s)} \rangle - \langle \ell(h, h^{(s)}), \mu^{(s)} \rangle + \langle \ell(h, h^{(u)}), \mu^{(u)} \rangle \\ &= R^{(s)}(h) + (\langle \ell(h, h^{(u)}), \mu^{(u)} \rangle - \langle \ell(h, h^{(s)}), \mu^{(u)} \rangle) + (\langle \ell(h, h^{(s)}), \mu^{(u)} \rangle - \langle \ell(h, h^{(s)}), \mu^{(s)} \rangle) \\ &\leq R^{(s)}(h) + \langle \ell(h^{(u)}, h^{(s)}), \mu^{(u)} \rangle + \langle \ell(h, h^{(s)}), \mu^{(u)} - \mu^{(s)} \rangle \end{aligned} \quad (20)$$

where (20) follows from the triangle inequality  $\ell(h, h^{(u)}) \leq \ell(h, h^{(s)}) + \ell(h^{(s)}, h^{(u)})$  and because  $\ell(h^{(s)}, h^{(u)}) = \ell(h^{(u)}, h^{(s)})$ .

In an analogous fashion, it is possible to show that:

$$R^{(u)}(h) \leq R^{(s)}(h) + \langle \ell(h^{(u)}, h^{(s)}), \mu^{(s)} \rangle + \langle \ell(h, h^{(u)}), \mu^{(u)} - \mu^{(s)} \rangle. \quad (21)$$

Let  $\mathbf{z} = f(\mathbf{x})$ . Since  $f$  is invertible,  $\mathbf{x} = f^{-1}(\mathbf{z})$ . The third term in the right-hand side of (21) can be bounded as follows.

$$\begin{aligned} &\langle \ell(h, h^{(u)}), \mu^{(u)} - \mu^{(s)} \rangle \\ &= \langle \ell(g \circ f, g^{(u)} \circ f^{(u)}), \mu^{(u)} - \mu^{(s)} \rangle \\ &= \mathbb{E}_{\mathbf{x} \sim \mu^{(u)}} [\ell(g \circ f(\mathbf{x}), g^{(u)} \circ f^{(u)}(\mathbf{x}))] - \mathbb{E}_{\mathbf{x} \sim \mu^{(s)}} [\ell(g \circ f(\mathbf{x}), g^{(u)} \circ f^{(u)}(\mathbf{x}))] \\ &= \mathbb{E}_{\mathbf{z} \sim f_{\#}\mu^{(u)}} [\ell(g(\mathbf{z}), g^{(u)} \circ f^{(u)} \circ f^{-1}(\mathbf{z}))] - \mathbb{E}_{\mathbf{z} \sim f_{\#}\mu^{(s)}} [\ell(g(\mathbf{z}), g^{(u)} \circ f^{(u)} \circ f^{-1}(\mathbf{z}))] \\ &= \langle \ell(g, g^{(u)} \circ f^{(u)} \circ f^{-1}), f_{\#}\mu^{(u)} - f_{\#}\mu^{(s)} \rangle \\ &\leq L \langle 1, |f_{\#}\mu^{(u)} - f_{\#}\mu^{(s)}| \rangle \end{aligned} \quad (22)$$

where (22) follows from the assumption that the loss function is bounded by a positive number  $L$  and the fact that  $f_{\#}\mu^{(u)} - f_{\#}\mu^{(s)} \leq |f_{\#}\mu^{(u)} - f_{\#}\mu^{(s)}|$ .

Combining (21) and (22) we get,

$$R^{(u)}(h) \leq R^{(s)}(h) + \langle \ell(h^{(u)}, h^{(s)}), \mu^{(s)} \rangle + L \langle 1, |f_{\#}\mu^{(u)} - f_{\#}\mu^{(s)}| \rangle. \quad (23)$$

By similar reasoning, from (20),

$$R^{(u)}(h) \leq R^{(s)}(h) + \langle \ell(h^{(u)}, h^{(s)}), \mu^{(u)} \rangle + L \langle 1, |f_{\#}\mu^{(u)} - f_{\#}\mu^{(s)}| \rangle. \quad (24)$$

The proof of Lemma 1 now follows by combining (23) and (24) and noting that  $\sigma^{(u,s)} = \min(\langle \ell(h^{(u)}, h^{(s)}), \mu^{(u)} \rangle, \langle \ell(h^{(u)}, h^{(s)}), \mu^{(s)} \rangle)$ , and  $\langle 1, |f_{\#}\mu^{(u)} - f_{\#}\mu^{(s)}| \rangle = \|f_{\#}\mu^{(u)} - f_{\#}\mu^{(s)}\|_1$ .

### A.3 Extend proof of Lemma 1 for nearly invertible representation maps

The proof of Lemma 1 requires that the representation map  $f$  is exactly invertible. However, this restricted condition can be relaxed. In practice, a function is called nearly invertible if there exists a reconstruction function with a sufficiently low reconstruction error. Based on the definition of nearly invertible maps, we aim to construct a similar upper bound as in Lemma 1. Now, assume that the representation map  $f$  is nearly invertible i.e., there exists a function  $s : \mathbb{R}^{d'} \rightarrow \mathbb{R}^d$  such that if  $f(\mathbf{x}) = \mathbf{z}$  then  $|\mathbf{x} - s(\mathbf{z})| \leq \delta \forall \mathbf{z}$  where  $\delta$  is a small positive constant.

Next, we assume that  $h^{(u)}$  is  $K$ -Lipschitz continuous. Hence,  $h^{(u)}(s(\mathbf{z})) - K\delta \leq h^{(u)}(\mathbf{x}) \leq h^{(u)}(s(\mathbf{z})) + K\delta$ .

In addition, we also assume that the cost function  $\ell(\cdot, \cdot)$  is  $Q$ -Lipschitz continuous i.e.,  $\ell(a, b) - Q|\gamma| \leq \ell(a, b + \gamma) \leq \ell(a, b) + Q|\gamma|$ . Thus,

$$\begin{aligned}
& \langle \ell(h, h^{(u)}), \mu^{(u)} - \mu^{(s)} \rangle \\
&= \langle \ell(g \circ f, g^{(u)} \circ f^{(u)}), \mu^{(u)} - \mu^{(s)} \rangle \\
&= \mathbb{E}_{\mathbf{x} \sim \mu^{(u)}} [\ell(g \circ f(\mathbf{x}), h^{(u)}(\mathbf{x}))] - \mathbb{E}_{\mathbf{x} \sim \mu^{(s)}} [\ell(g \circ f(\mathbf{x}), h^{(u)}(\mathbf{x}))] \\
&\leq \max \left\{ \mathbb{E}_{\mathbf{z} \sim f_\# \mu^{(u)}} [\ell(g(\mathbf{z}), h^{(u)}(s(\mathbf{z})) + K\delta)], \mathbb{E}_{\mathbf{z} \sim f_\# \mu^{(u)}} [\ell(g(\mathbf{z}), h^{(u)}(s(\mathbf{z})) - K\delta)] \right\} \\
&- \min \left\{ \mathbb{E}_{\mathbf{z} \sim f_\# \mu^{(s)}} [\ell(g(\mathbf{z}), h^{(u)}(s(\mathbf{z})) + K\delta)], \mathbb{E}_{\mathbf{z} \sim f_\# \mu^{(s)}} [\ell(g(\mathbf{z}), h^{(u)}(s(\mathbf{z})) - K\delta)] \right\} \\
&\leq \mathbb{E}_{\mathbf{z} \sim f_\# \mu^{(u)}} [\ell(g(\mathbf{z}), g^{(u)} \circ f^{(u)}(s(\mathbf{z})))] - \mathbb{E}_{\mathbf{z} \sim f_\# \mu^{(s)}} [\ell(g(\mathbf{z}), g^{(u)} \circ f^{(u)}(s(\mathbf{z})))] \\
&+ \mathbb{E}_{\mathbf{z} \sim f_\# \mu^{(u)}} [QK\delta] + \mathbb{E}_{\mathbf{z} \sim f_\# \mu^{(s)}} [QK\delta] \\
&\leq \langle \ell(g, g^{(u)}), f_\# \mu^{(u)} - f_\# \mu^{(s)} \rangle + QK\delta + QK\delta \\
&\leq L \langle 1, |f_\# \mu^{(u)} - f_\# \mu^{(s)}| \rangle + 2QK\delta
\end{aligned} \tag{25}$$

where the fourth inequality due to the assumption that  $\ell(\cdot, \cdot)$  is a distance metric, both  $g(\cdot)$  and  $g^{(u)}(\cdot)$  map  $\mathbf{z}$  to 1-dimension space and the fact that  $h^{(u)}(s(\mathbf{z})) - K\delta \leq h^{(u)}(\mathbf{x}) \leq h^{(u)}(s(\mathbf{z})) + K\delta$ , the fifth inequality due to  $\ell(\cdot, \cdot)$  is  $Q$ -Lipschitz, and the last inequality due to  $\ell(\cdot, \cdot)$  is bounded by  $L$ . In comparison to the original result in Lemma 1, one more term  $(2QK\delta)$  is introduced in the upper bound if the representation map is nearly invertible. If  $\delta = 0, \forall \mathbf{z}$ , or in other words, the representation map is exactly invertible, then the extra term  $2QK\delta$  is, of course, zero.

### A.4 Proof of Lemma 3

From Pinsker's inequality [Berend et al., 2014, Csiszár and Körner, 2011], the  $L^1$  distance can be bounded by Kullback–Leibler (KL) divergence as follows:

$$\|\mu - \nu\|_1^2 \leq 2d_{KL}(\mu, \nu) \tag{26}$$

where  $\|\mu - \nu\|_1$  and  $d_{KL}(\mu, \nu)$  denote  $L^1$  distance and Kullback–Leibler divergence between two distributions  $\mu$  and  $\nu$ , respectively. Since  $\|\mu - \nu\|_1 = \|\nu - \mu\|_1$ , using Pinsker's inequality for  $(\mu, \nu)$  and  $(\nu, \mu)$ ,

$$2\|\mu - \nu\|_1^2 = \|\mu - \nu\|_1^2 + \|\nu - \mu\|_1^2 \leq 2d_{KL}(\mu, \nu) + 2d_{KL}(\nu, \mu) \tag{27}$$

which is equivalent to,

$$\|\mu - \nu\|_1 \leq \sqrt{d_{KL}(\mu, \nu) + d_{KL}(\nu, \mu)}. \quad (28)$$

Next, if  $\mu$  and  $\nu$  are  $(c_1, c_2)$ -regular distributions, their Kullback–Leibler divergences can be bounded by their Wasserstein-2 distance as follows (please see equation (10), Proposition 1 in [Polyanskiy and Wu, 2016]),

$$d_{KL}(\mu, \nu) + d_{KL}(\nu, \mu) \leq 2 \left( \frac{c_1}{2} \sqrt{\mathbb{E}_{\mathbf{u} \sim \mu} [\|\mathbf{u}\|_2^2]} + \frac{c_1}{2} \sqrt{\mathbb{E}_{\mathbf{v} \sim \nu} [\|\mathbf{v}\|_2^2]} + c_2 \right) \quad [\mathbb{W}_2(\mu, \nu)]. \quad (29)$$

Combining (28) and (29),

$$\|\mu - \nu\|_1 \leq \sqrt{c_1 \left( \sqrt{\mathbb{E}_{\mathbf{u} \sim \mu} [\|\mathbf{u}\|_2^2]} + \sqrt{\mathbb{E}_{\mathbf{v} \sim \nu} [\|\mathbf{v}\|_2^2]} \right) + 2c_2} \quad [\mathbb{W}_2(\mu, \nu)]^{1/2}. \quad (30)$$

## A.5 Proof of Theorem 1

Under the assumption that  $f_{\#}\mu^{(s)}$  and  $f_{\#}\mu^{(u)}$  are  $(c_1, c_2)$ -regular  $\forall s = 1, 2, \dots, S$ , from Lemma 3,

$$\|f_{\#}\mu^{(u)} - f_{\#}\mu^{(s)}\|_1 \leq \sqrt{c_1 \left( \sqrt{\mathbb{E}_{\mathbf{x} \sim \mu^{(s)}} [\|f(\mathbf{x})\|_2^2]} + \sqrt{\mathbb{E}_{\mathbf{x} \sim \mu^{(u)}} [\|f(\mathbf{x})\|_2^2]} \right) + 2c_2} \quad [\mathbb{W}_2(f_{\#}\mu^{(u)}, f_{\#}\mu^{(s)})]^{1/2}. \quad (31)$$

Let:

$$C := \max_{s \in \{1, \dots, S\}} \sqrt{c_1 \left( \sqrt{\mathbb{E}_{\mathbf{x} \sim \mu^{(s)}} [\|f(\mathbf{x})\|_2^2]} + \sqrt{\mathbb{E}_{\mathbf{x} \sim \mu^{(u)}} [\|f(\mathbf{x})\|_2^2]} \right) + 2c_2}. \quad (32)$$

Multiplying (31) by  $\lambda^{(s)}$  and summing over all  $s$  we get:

$$\sum_{s=1}^S \lambda^{(s)} \|f_{\#}\mu^{(u)} - f_{\#}\mu^{(s)}\|_1 \leq C \sum_{s=1}^S \lambda^{(s)} [\mathbb{W}_2(f_{\#}\mu^{(u)}, f_{\#}\mu^{(s)})]^{1/2}. \quad (33)$$

By Jensen's inequality,

$$\sum_{s=1}^S \lambda^{(s)} [\mathbb{W}_2(f_{\#}\mu^{(u)}, f_{\#}\mu^{(s)})]^{1/2} \leq \left[ \sum_{s=1}^S \lambda^{(s)} \mathbb{W}_2^2(f_{\#}\mu^{(u)}, f_{\#}\mu^{(s)}) \right]^{1/4}. \quad (34)$$

From (33) and (34),

$$\sum_{s=1}^S \lambda^{(s)} \|f_{\#}\mu^{(u)} - f_{\#}\mu^{(s)}\|_1 \leq C \left[ \sum_{s=1}^S \lambda^{(s)} \mathbb{W}_2^2(f_{\#}\mu^{(u)}, f_{\#}\mu^{(s)}) \right]^{1/4}. \quad (35)$$

Finally, combining the upper bound in Lemma 2 and (35), the proof follows.